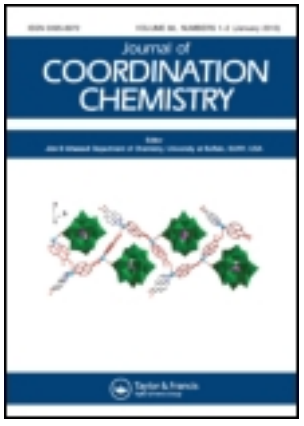

Journal of Coordination Chemistry
Publication details, including instructions for authors and subscription information:
http://www.tandfonline.com/loi/gcoo20

Syntheses, structures, and properties of two coordination polymers based on 5-methoxyisophthalate and flexible dipyridines

Xiaoju Li[a], Guangchao Ma[a] & Xiahong Xu[a]
[a] Fujian Key Laboratory of Polymer Materials, College of Materials Science and Engineering, College of Chemistry and Chemistry Engineering, Fujian Normal University, Fuzhou, China
Accepted author version posted online: 07 Aug 2013.Published online: 24 Sep 2013.

To cite this article: Xiaoju Li, Guangchao Ma & Xiahong Xu (2013) Syntheses, structures, and properties of two coordination polymers based on 5-methoxyisophthalate and flexible dipyridines, Journal of Coordination Chemistry, 66:18, 3249-3260, DOI: 10.1080/00958972.2013.832759

To link to this article: http://dx.doi.org/10.1080/00958972.2013.832759

Journal of Coordination Chemistry, 2013
Vol. 66, No. 18, 3249–3260, http://dx.doi.org/10.1080/00958972.2013.832759

Syntheses, structures, and properties of two coordination polymers based on 5-methoxyisophthalate and flexible dipyridines

XIAOJU LI*, GUANGCHAO MA and XIAHONG XU

Fujian Key Laboratory of Polymer Materials, College of Materials Science and Engineering, College of Chemistry and Chemistry Engineering, Fujian Normal University, Fuzhou, China

(*Received 17 October 2012; accepted 16 July 2013*)

Hydrothermal reactions of 5-methoxyisophthalic acid (MeO-H_2ip), 1,3-di(4-pyridyl)propane (bpp) with $Cd(NO_3)_2{\cdot}4H_2O$ and $Ni(NO_3)_2{\cdot}6H_2O$ produced $[Cd_2(MeO\text{-}ip)_2(bpp)_2]_n{\cdot}nH_2O$ (**1**) and $[Ni(MeO\text{-}ip)(bpp)(H2O)]_n{\cdot}nH_2O$ (**2**), respectively. Complex **1** is a 2-D layer consisting of dinuclear Cd(II)-carboxylate units, two carboxylates of MeO-ip adopt μ_2,η^2-bridging and chelating modes. MeO-ip bridges three Cd(II) ions to form a 1-D $[Cd_2(MeO\text{-}ip)_2]_n$ chain, which is further extended into a 2-D layer by bpp in a *trans,trans*-conformation. However, two carboxylates of MeO-ip in **2** are monodentate and chelating to link Ni(II) into a 1-D $[Ni(MeO\text{-}ip)]_n$ chain with bpp in a *trans-gauche* conformation connecting $[Ni(MeO\text{-}ip)]_n$ chains into a two-fold interpenetrating 3-D network. Coordinated water and carboxylate oxygen from different MeO-ip form strong hydrogen bonds. The frameworks of **1** and **2** are stable below 250 and 300 °C, respectively. Luminescence indicates that **1** shows maximum emission at 375 and 450 nm upon excitation at 320 nm. Magnetic measurement of **2** suggests the presence of ferromagnetic interactions in **2**.

Keywords: Cadmium; Coordination polymer; Crystal structure; Luminescence; Magnetism

1. Introduction

Design and synthesis of metal–organic frameworks (MOFs) have attracted considerable interest in supramolecular chemistry and crystal engineering because of their intriguing structures and potential applications in luminescence, magnetism, heterogeneous catalysis, gas adsorption, and gas separation [1–3]. Progress has been made in the synthesis and structural characterization of MOFs. However, it is still a challenge to control synthesis of MOFs with desirable structures and functions [4, 5]. Structural characteristics of ligands, the coordination geometry of metal ions, different counter ions, solvents, temperatures, and pH have influence on the assembly of organic ligands and metal ions [6–9]. Carboxylate ligands are frequently used for their versatile coordination modes and strong coordination ability to transition metal ions. The effect of counter anions on the assembly of carboxylate and metal ions may be mitigated [10].

*Corresponding author. Email: xiaojuli@fjnu.edu.cn

Two carboxylates in isophthalate and its derivatives are predisposed to 120° at the central phenyl ring, providing constrained and proper binding directions to metal ions [11–13]. Assembly with metal ions generated various coordination polymers, ranging from discrete macrocycles, molecular capsules, 1-D chains to 2-D layers and 3-D networks [14–16]. Structures and properties of the target complexes have also been affected by an electronic and steric character of the five-position substituent [17, 18].

Exo-bidentate *N*-containing ligands have also been employed in the construction of MOFs [19, 20]; 1,3-di(4-pyridyl)propane (bpp) is a promising candidate, possessing *trans-trans* and *trans-gauche* conformations based on the relative orientation of the $(CH_2)_3$ spacer (scheme 1). The flexible nature of spacer allows it to freely rotate to meet coordination geometries of metal ions in the assembly process, resulting in MOFs with beautiful structures and useful properties [21, 22].

In previous study, we primarily focused on the construction of MOFs using *exo*-bidentate *N*-containing ligands and 5-hydroxyisophthalate [22, 23], in which the mixed ligands play different roles in the structural construction of final products. 5-Hydroxyisophthalate usually bridges metal ions to generate charge neutral frameworks, the *N*-containing ligands may further extend the metal carboxylate frameworks into higher dimensional architectures. The hydroxyl group in 5-hydroxyisophthalate does not take part in coordination, but can serve as a hydrogen bond donor to form strong hydrogen bonding interactions with carboxylate oxygens. As a continuation of our research on the influence of systematic variations of the five-position substituents of isophthalate on the structures and properties of MOFs, we examine hydroxyl alkylation in 5-hydroxyisophthalate to produce MOFs, inhibiting hydrogen bonds from the hydroxyl group. Herein, we report the synthesis and characterization of two MOFs from 5-methoxyisophthalate (MeO-ip) and bpp, $[Cd_2(MeO\text{-}ip)_2(bpp)_2]_n \cdot nH_2O$ (**1**) and $[Ni(MeO\text{-}ip)(bpp)(H_2O)]_n \cdot nH_2O$ (**2**).

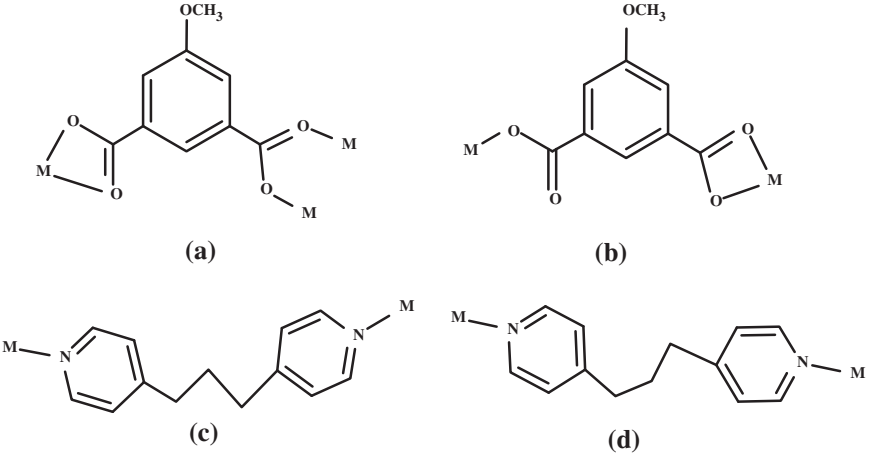

Scheme 1. Coordination modes of MeO-ip and bpp.

2. Experimental

2.1. *Materials and physical measurements*

MeO-H_2ip was synthesized according to the literature method [24]. All other chemicals were purchased from commercial suppliers and used as received. IR spectra (KBr pellets) were recorded on a Magna750 FT-IR spectrophotometer from 400 to 4000 cm^{-1}. Powder X-ray diffraction data were recorded on a PANaytical X'pert pro X-ray diffractometer with graphite-monochromated CuKα radiation (λ = 1.542 Å). Thermal stability studies were carried out on a NETSCHZ STA 449C thermoanalyzer at a heating rate of 10 °C min^{-1} under N_2. Fluorescence spectroscopy was performed on an Edinburgh Analytical Instrument FLS920. C, H, and N elemental analyses were determined on an EA1110 CHNS-0CE element analyzer.

2.2. *Synthesis of $[Cd_2(MeO\text{-}ip)_2(bpp)_2]_n \cdot nH_2O$ (1)*

A mixture of MeO-H_2ip (0.25 mM, 49.0 mg), bpp (0.25 mM, 49.6 mg), $Cd(NO_3)_2 \cdot 4H_2O$ (0.25 mM, 77.1 mg), and aqueous NaOMe (0.5 mL, 1 M) in H_2O (10 mL) was placed in a Teflon-lined stainless steel vessel (25 mL) and then heated at 130 °C for 3 days, followed by slowly cooling to room temperature at a rate of 3 °C h^{-1}. Colorless block crystals of **1** were obtained. Yield: 25.4 mg (20%). Elemental analysis (%): $C_{22}H_{21}CdN_2O_{5.5}$ (513.82): C 51.43, H 4.12, N 5.45; found C 51.63, H 4.02, N 5.61. IR (KBr, cm^{-1}): 3434 (w), 2943 (vw), 1606 (s), 1565 (vs), 1440 (m), 1365 (vs), 1313 (w), 1230 (vw), 1050 (m), 924 (vw), 774 (m), 732 (m), 606 (vw), 504 (vw).

2.3. *Synthesis of $[Ni(MeO\text{-}ip)(bpp)(H_2O)]_n \cdot nH_2O$ (2)*

Complex **2** was synthesized in a similar procedure as described for **1** except using $Ni(NO_3)_2 \cdot 6H_2O$ instead of $Cd(NO_3)_2 \cdot 4H_2O$; green block crystals of **2** were obtained. Yield: 42.4 mg (36%). Elemental analysis (%): calcd for $C_{22}H_{24}N_2O_7Ni$ (487.13): C 54.24, H 4.97, N 5.75; found C 54.66, H 4.86, N 5.90. IR (KBr, cm^{-1}): 3407 (w), 2937 (vw), 1616 (vs), 1574 (s), 1445 (s), 1371 (vs), 1319 (w), 1217 (w), 1121 (vw), 1055 (m), 1007 (vw), 768 (m), 708 (m), 570 (vw), 500 (vw).

2.4. *Crystallographic data and structure determination*

Single crystals of **1** and **2** were mounted on a glass fiber for X-ray diffraction analysis. Data were collected on a Rigaku AFC7R equipped with graphite-monochromated Mo-Kα radiation (λ = 0.71073 Å) from a rotating generator at 293 K. Intensities were corrected for LP factors and empirical absorption using the ψ scan technique. The structures were solved by direct methods and refined on F^2 with full-matrix least-squares techniques using Siemens *SHELXTL* version 5 package of crystallographic software [25]. All nonhydrogen atoms were refined anistropically. Hydrogens of water in **2** were located from the difference Fourier map and refined isotropically. The positions of other hydrogens were generated geometrically (C–H bond fixed at 0.96 Å), assigned isotropic thermal parameters, and allowed to ride on their parent carbons before the final cycle of refinement. Crystal data as well as details of data collection and refinement for **1** and **2** are summarized in table 1.

Table 1. Crystal data and structure refinement results for **1** and **2**.

Complexes	**1**	**2**
Empirical formula	$C_{22}H_{21}CdN_2O_{5.5}$	$C_{22}H_{24}NiN_2O_7$
Formula weight	513.81	487.14
Crystal system	Monoclinic	Monoclinic
Space group	*P2(1)/c*	*C2/c*
a (Å)	10.1953(13)	14.419(13)
b (Å)	17.293(3)	18.307(15)
c (Å)	15.743(2)	16.937(15)
β (°)	125.668(10)	104.286(16)
Volume (Å^3)	2254.9(6)	4333(7)
Z	4	8
ρ_{Calcd} (mg·m^{-3})	1.513	1.494
μ (mm^{-1})	1.005	0.943
F (0 0 0)	1036	2032
Reflections collected	17,336	16,541
Unique reflections	5120	4912
Parameters	281	290
R_{int}	0.0527	0.1032
S on F^2	1.081	1.007
R_1 ($I > 2\sigma(I)$)[a]	0.0571	0.0740
${}_wR_2$($I > 2\times\sigma(I)$)[b]	0.1362	0.1805
R_1 (all data)[a]	0.0834	0.1235
${}_wR_2$ (all data)[b]	0.1525	0.2146
$\Delta\rho_{max}$ and $\Delta\rho_{min}$ [e·Å^{-3}]	0.864 and −0.588	1.107 and −0.734

[a]$R_1 = \sum||F_o| - |F_c||/\sum|F_o|$; [b]$wR_2 = \sum[w(F_o^2-F_c^2)^2]/\sum[w(F_o^2)^2]^{1/2}$.

Selected bond distances and angles are given in table 2. Crystallographic data of **1** and **2** have been deposited in the Cambridge Crystallographic Data Centre as supplementary publication with CCDC number 871,765–871,766.

Table 2. Selected bond lengths (Å) and angles (°) for **1** and **2**.

1			
Cd1–N1	2.306(4)	Cd1–N2C	2.410(4)
Cd1–O1	2.231(4)	Cd1–O2B	2.384(4)
Cd1–O3A	2.368(4)	Cd1–O4A	2.392(4)
O1–Cd1–N1	127.39(15)	O1–Cd1–O3A	140.36(13)
N1–Cd1–O4A	146.64(14)	O2B–Cd1–N2C	177.48(14)
N1–Cd1–O3A	91.50(14)	O1–Cd1–O2B	95.63(13)
N1–Cd1–O2A	86.89(15)	O3A–Cd1–O2B	93.65(13)
O1–Cd1–O4A	85.87(13)	O3A–Cd1–O4A	55.20(12)
O2B–Cd1–O4A	92.90(14)	O1–Cd1–N2C	84.17(15)
N1–Cd1–N2C	91.23(16)	O3A–Cd1–N2C	88.08(15)
O4A–Cd1–N2C	89.59(15)		
2			
Ni1–N1	2.076(4)	Ni1–N2B	2.127(4)
Ni1–O4A	2.027(3)	Ni1–O1W	2.074(4)
Ni1–O1	2.097(3)	Ni1–O2	2.256(4)
O4A–Ni1–O1	175.33(12)	O1W–Ni1–N2B	172.46(13)
N1–Ni1–O2	153.80(13)	O4A–Ni1–O2	115.28(13)
O4A–Ni1–N1	90.78(16)	O4A–Ni1–O1W	86.99(13)
N1–Ni1–O1W	92.48(13)	N1–Ni1–O1	93.33(15)
O1W–Ni1–O1	90.63(12)	O4A–Ni1–N2B	91.58(14)
N1–Ni1–N2B	95.31(15)	O1–Ni1–N2B	90.24(13)
N2B–Ni1–O2	87.01(14)	O1–Ni1–O2	60.52(12)
O1W–Ni1–O2	86.58(12)		

Symmetry transformations used to generate equivalent atoms for **1**: (A) $x-1$, y, z; (B) $-x-1$, $-y$, $-z+1$; (C) $x-1$, y, $z-1$; for **2**: (A) x, $-y+1$, $z-1/2$; (B) $x+1/2$, $-y+3/2$, $z+1/2$.

3. Results and discussion

3.1. *Structural description of $[Cd_2(MeO\text{-}ip)_2(bpp)_2]_n \cdot nH_2O$ (1)*

Single-crystal X-ray analysis showed that **1** is a 2-D layer consisting of dinuclear Cd(II)-carboxylate units. As shown in figure 1(a), Cd1 has distorted octahedral coordination geometry, defined by four carboxylate oxygens and two pyridyl nitrogens. The equatorial plane is defined by one pyridyl nitrogen from bpp, two chelating carboxylate oxygens and one μ_2,η^2-carboxylate *cis*-oxygen from a different MeO-ip. The mean deviation of Cd(II) from the equatorial plane is 0.074 Å. One pyridyl nitrogen from the other bpp and one μ_2,η^2-carboxylate oxygen occupy axial positions with the N2C-Cd1-O2B bond angle of 177.45(14)°. As shown in scheme 1(a), MeO-ip uses its μ_2,η^2-bridging and chelating carboxylates to bridge three Cd(II) ions. The twisting angle of the former with the central phenyl ring is 8.7°, smaller than that of the latter with the phenyl ring (21.2°). Two μ_2,η^2-carboxylates from different MeO-ip bridge equivalently two Cd(II) ions resulting in a dinuclear unit with the crystallographic inversion center at the middle of the Cd1-Cd1B core, the Cd1···Cd1B distance is 4.319 Å, much longer than those from paddlewheel dinuclear Cd(II)-tetracarboxylate units [26]. MeO-ip links adjacent dinuclear units into a 1-D $[Cd_2(MeO\text{-}ip)_2]_n$ chain (figure 1(b)) with closest Cd(II)···Cd(II) separation between dinuclear units of 7.851 Å. The *exo*-bidenate bpp adopts a *trans-trans* conformation (scheme 1(c)), linking dinuclear Cd(II)-carboxylate units into a macrocycle (figure 1(c)). In the macrocycle, the nearest Cd(II)···Cd(II) separation bridged by bpp is 10.737 Å. Twisting between two pyridyl rings in bpp is observed with dihedral angle of 70.8°, while the C15–C16–C17 bond angle in the $(CH_2)_3$ spacer is 115.3(6)°. The flexible rotation and bending of C15–C16–C17 enable the two pyridyl rings to meet the requirement of coordination geometries of the metal centers for assembly of **1**. As shown in figure 1(d), fusing the macrocycles and 1-D chains results in the formation of a 2-D layer, which is

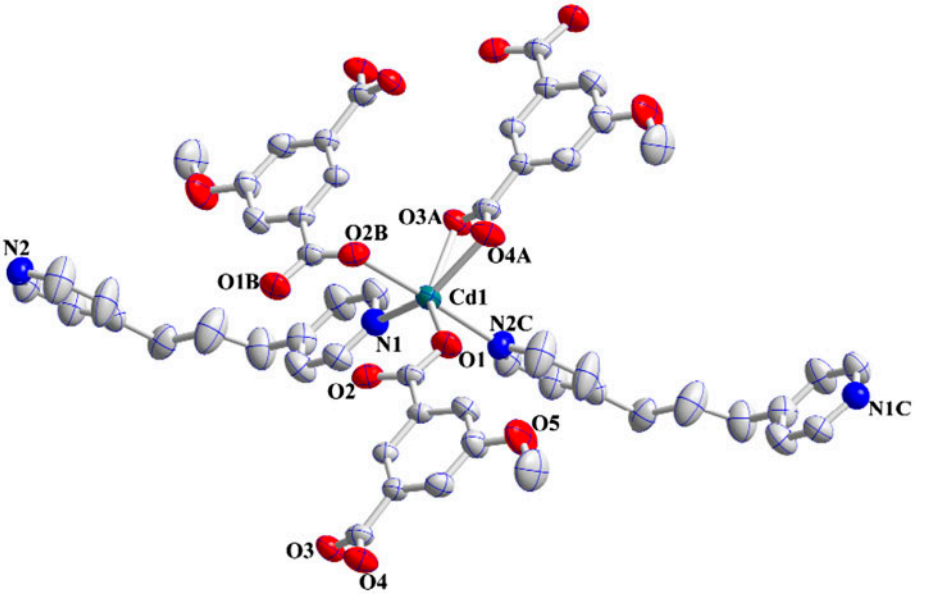

Figure 1(a). The coordination environment of Cd(II) in **1** with the thermal ellipsoids at 50% probability.

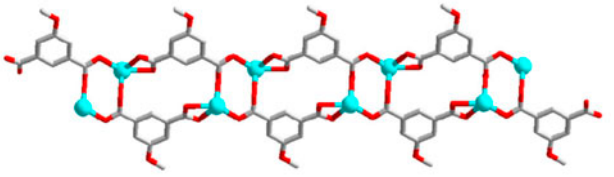

Figure 1(b). View of 1-D $[Cd_2(MeO\text{-}ip)_2]_n$ chain in **1**.

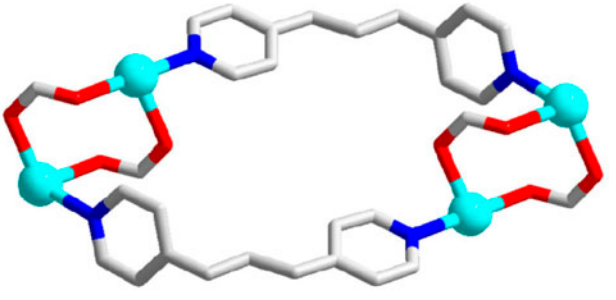

Figure 1(c). View of a macrocycle constructed through bpp bridging dinuclear Cd(II)-carboxylate units in **1**.

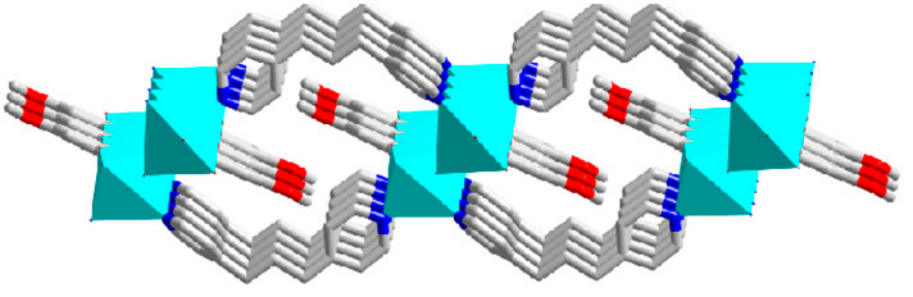

Figure 1(d). View of a 2-D layer in **1**.

much different from the reported cadmium(II) complex of 5-hydroxyisophthalate and bpp [27]. The 2-D layers are stacked in a spatial offset mode with crystalline water molecules located between the adjacent layers as guest molecules (figure 1(e)).

3.2. *Structural description of $[Ni(MeO\text{-}ip)(bpp)(H_2O)]_n \cdot nH_2O$ (2)*

Complex **2** crystallizes in the monoclinic space group *C2/c*, is a two-fold interpenetrating 3-D network consisting of mononuclear Ni(II) nodes. As shown in figure 2(a), the coordination environment of Ni1 is a distorted octahedral geometry, coordinated by three carboxylate oxygens, two pyridyl nitrogens, and one water. The equatorial plane is defined by one pyridyl nitrogen from bpp, two chelating carboxylate oxygens, and one monodentate carboxylate oxygen from different MeO-ip. The mean deviation of Ni(II) from the

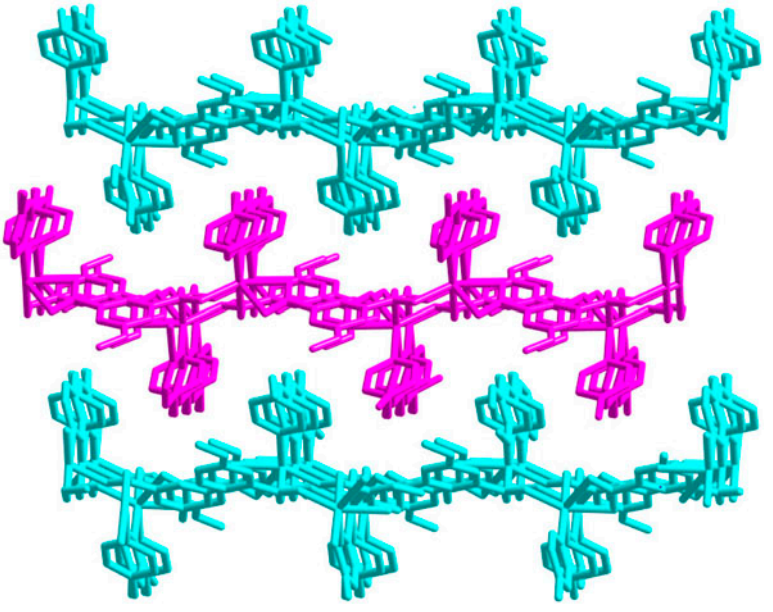

Figure 1(e). Packing diagram viewed along the *c*-axis; waters were omitted for clarity in **1**.

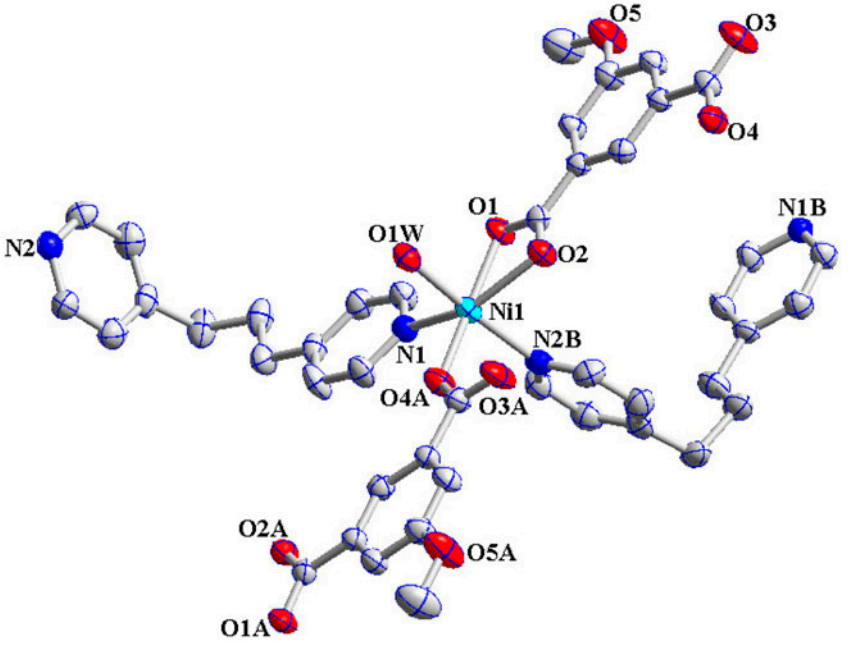

Figure 2(a). The coordination environment of Ni(II) in **2** with the thermal ellipsoids at 50% probability.

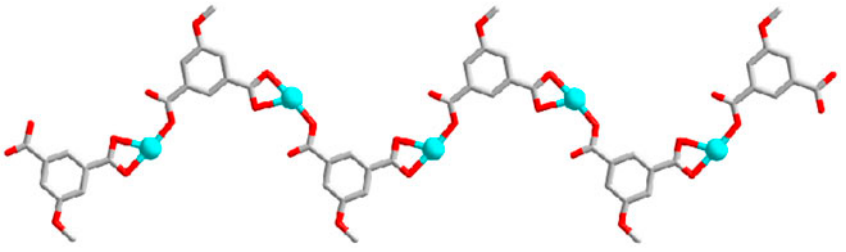

Figure 2(b). View of 1-D $[Ni(MeO\text{-}ip)]_n$ chain in **2**.

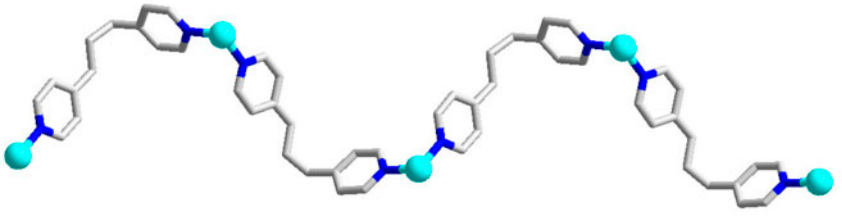

Figure 2(c). View of 1-D chain constructed from Ni(II) ions bridged by bpp ligands.

equatorial plane is 0.0413 Å. Pyridyl nitrogen from the other bpp and one coordinated water occupy axial positions with the O1 W–Ni1-N2B bond angle being 172.46(13)°. The Ni–N/O bond lengths are 2.027(3)–2.254(3) Å. Different from **1**, two carboxylates in MeO-ip adopt chelating and monodentate modes (scheme 1(b)), which are almost coplanar with the central phenyl ring with the twisting angles with phenyl being 2.1° and 1.6°, respectively. MeO-ip bridges adjacent Ni(II) ions to form a 1-D $[Ni(MeO\text{-}ip)]_n$ chain (figure 2(b)), in which the closest Ni(II)···Ni(II) separation across MeO-ip is 8.974 Å. In **2** bpp adopts a *trans-gauche* conformation (scheme 1(d)) with the dihedral angle between two pyridyl rings of 81.8°, larger than that in **1**, while the C6–C7–C8 bond angle of 112.1(5)° in the $(CH_2)_3$ spacer is lower than in **1**. The bpp bridges two adjacent Ni(II) ions to form a 1-D chain (figure 2(c)). The Ni···Ni separation across bpp is 11.480 Å, longer than that in **1**. Fusing of two types of 1-D chains generates a 3-D network (figure 2(d)). Crystalline waters are located in the 3-D network as guest molecules through hydrogen bonds [O(2 W)–H(2 W)···O3^{i} 2880(11) Å, symmetry code: (i) $x - 1/2$, $-y + 3/2$, $z - 1/2$]. Potential voids are further filled via mutual interpenetration of two equivalent frameworks, generating a two-fold interpenetrating 3-D framework (figure 2(e)). Strong hydrogen bonds between coordination waters and carboxylate oxygens of different MeO-ip from the other 3-D network [O1 W–H1 WA···O3^{ii} 2.720(5) Å, O1W–H1WB···O2^{iii} 2.781(5) Å, symmetry code: (ii) $-x + 1$, y, $-z + 3/2$; $-x + 1$, $-y + 1$, $-z + 1$] are observed in the whole framework, the nearest Ni···Ni separation between the interpenetrating 3-D networks is 5.294 Å.

3.3. *X-ray powder diffraction*

In order to check the purity of **1** and **2**, their original samples were measured by X-ray powder diffraction at room temperature. As shown in figure S1, the peak positions of the

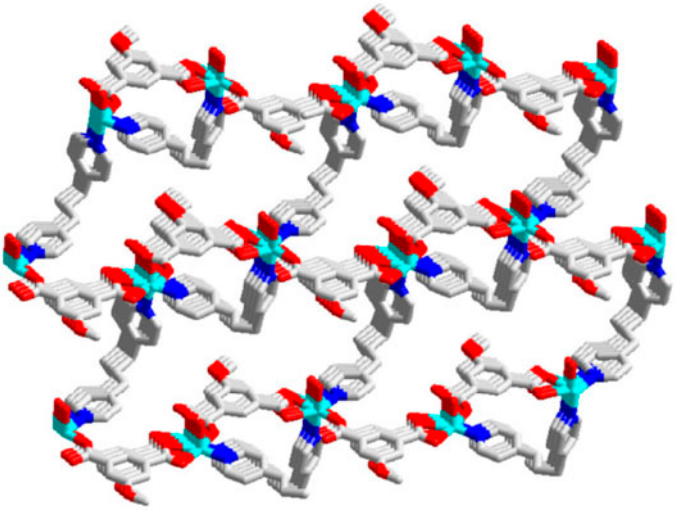

Figure 2(d). View of a 3-D network in **2**; waters were omitted for clarity.

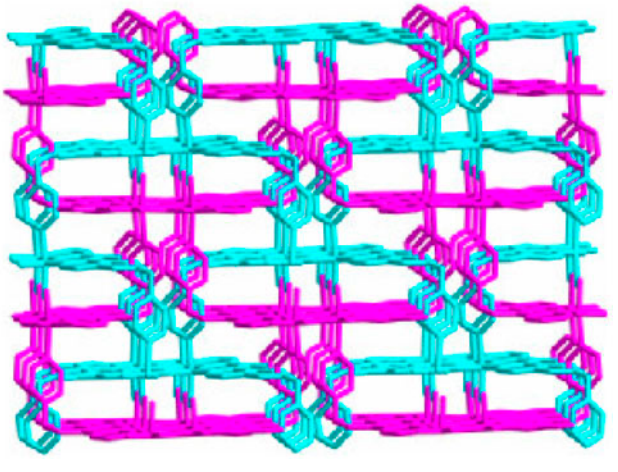

Figure 2(e). View of a two-fold interpenetrating 3-D network in **2**.

experimental patterns are in agreement with the simulated ones, indicating good purity of the complexes.

3.4. *Thermogravimetric analysis*

The thermal stabilities of **1** and **2** were investigated on polycrystalline samples under nitrogen. As shown in figure S2, thermogravimetric analysis (TGA) curve of **1** shows first weight loss of 1.56% before 135 °C, ascribed to the removal of crystalline water (Calcd 1.72%). Complex **1** was stable to 250 °C. The TGA curve of **2** indicates that the first

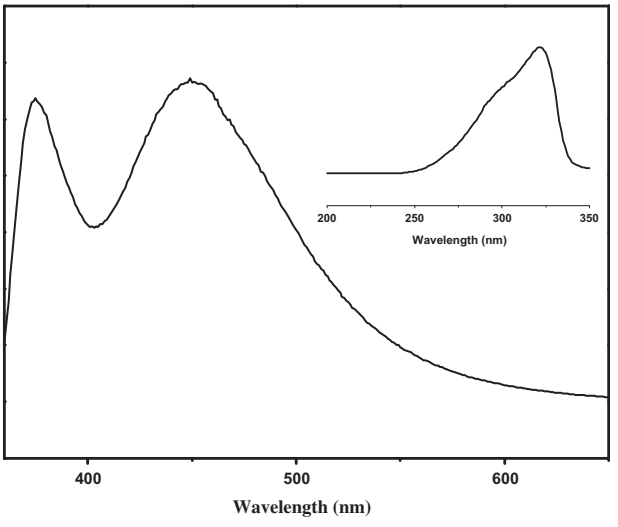

Figure 3. The fluorescent emission spectra and excitation spectra (inset) of **1**.

weight loss of 3.67% before 175 °C corresponds to loss of lattice waters (Calcd 3.70%) and the second weight loss of 3.78% from 175 and 300 °C is assigned as the removal of coordinated water (Calcd 3.70%); the framework begins to collapse after 300 °C.

3.5. *Photoluminescence*

Luminescence of **1** was studied in the solid state at room temperature. As shown in figure 3, **1** shows emission maxima at 375 and 450 nm upon excitation at 320 nm. As reported previously, free bpp has no luminescence from 300 to 800 nm upon excitation at

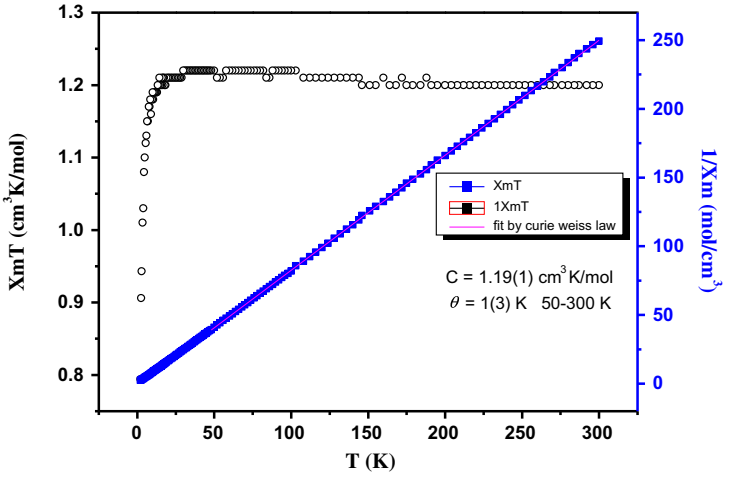

Figure 4. Temperature-dependent magnetic susceptibility in **2**.

300–450 nm at ambient temperature [28]. Free MeO-H_2ip exhibits the strongest emission peak at 407 nm upon excitation at 350 nm in the solid state at room temperature [29]. The emission of **1** is neither ligand-to-metal charge transfer nor metal-to-ligand charge transfer, and may be assigned to chelating or bridging carboxylates to Cd(II) [30–32], resulting in the variation of the rigidity and conjugation of MeO-ip.

3.6. *Magnetic property*

The temperature-dependent magnetic susceptibility data of **2** were measured at an applied magnetic field of 1000 Oe from 2 to 300 K. As shown in figure 4, the experimental value of $\chi_m T$ at 300 K is 1.20 emu K M^{-1} per formula unit, which is close to the theoretical value (1.21 emu K M^{-1}) of an uncoupled high-spin Ni(II) for g = 2.2 [33]. Upon cooling, $\chi_m T$ increases to a maximum of 1.22 emu K M^{-1} at 29.9 K, then sharply decreases to 0.794 emu K mol^{-1} at 2 K, which might be attributed to the presence of zero-field splitting of Ni(II). The magnetic behavior suggests the presence of ferromagnetic interactions in **2**. The temperature dependence of the reciprocal susceptibilities ($1/\chi_m$) obeys the Curie-Weiss law above 50 K with the positive Weiss constant θ = 1.27 K, which further supports the presence of ferromagnetic coupling in **2** and is typical for high-spin, six-coordinated Ni(II) complexes [34].

4. Conclusion

Two Cd(II) and Ni(II) MOFs based on MeO-ip and bpp have been hydrothermally synthesized and characterized. Cd(II) in **1** and Ni(II) in **2** are in distorted octahedral geometries. Complex **1** is a 2-D layer consisting of dinuclear Cd(II)-carboxylate units, while **2** is a two-fold interpenetrating 3-D network consisting of mononuclear Ni(II) nodes. Their structures are much different from counterparts constructed by 5-hydroxyisophthalate and bpp, probably because the methoxy instead of hydroxy in 5-hydroxyisophthalate prevents the formation of hydrogen bonds from hydroxyl. MeO-ip possesses different bridging modes, two carboxylates of MeO-ip in **1** adopt μ_2,η^2-bridging and chelating modes, while two carboxylates of MeO-ip in **2** function in monodentate and chelating modes. MeO-ip in **1** and **2** connects metal ions into 1-D chains; bpp in *trans-trans* and *trans-gauche* conformations further links 1-D chains into 2-D layer and 3-D network, respectively. The twisting angle between two pyridyl rings and the bond angle of $(CH_2)_3$ spacer in bpp is much different in **1** and **2**. This study shows the use of alkylated 5-hydroxyisophthalate and the flexible dipyridyl ligands is an effective strategy for the construction of MOFs. Further research will focus on the mixed use of other five-positioned alkylated hydroxyisophthalate and *exo*-bidentate nitrogen-containing ligands.

Acknowledgments

This work was supported by the National Natural Science Foundation of China (21001025), the Natural Science Foundation of Fujian Province (2010J05017), and Provincial Education Department of Fujian (JA12070).

References

[1] M.D. Allendorf, C.A. Bauer, R.K. Bhakta, R.J.T. Houk. *Chem. Soc. Rev.*, **38**, 1330 (2009).
[2] F.H. Cai, Y.Y. Ge, H.Y. Jia, S.S. Li, F. Sun, L.G. Zhang, Y.P. Cai. *Cryst. Eng. Comm.*, **13**, 67 (2011).
[3] X. Zhang, G.C. Ma, F.Z. Kong, Z.Y. Yu, R.H. Wang. *Inorg. Chem. Commun.*, **22**, 44 (2012).
[4] C. Hou, Q. Liu, Y. Lu, T. Okamura, P. Wang, M. Chen, W.Y. Sun. *Microporous Mesoporous Mater.*, **152**, 96 (2012).
[5] Y. Zhou, J.-N. Peng. *J. Coord. Chem.*, **66**, 2597 (2013).
[6] R.H. Wang, H.Y. Xu, Y. Guo, R.J. Sa, J.M. Shreeve. *J. Am. Chem. Soc.*, **132**, 11904 (2010).
[7] G.B. Che, J. Wang, B. Liu, X.Y. Li, C.B. Liu. *J. Coord. Chem.*, **62**, 302 (2009).
[8] B. Zheng, H. Dong, J. Bai, Y. Li, S. Li, M. Scheer. *J. Am. Chem. Soc.*, **130**, 7778 (2008).
[9] P. Kanoo, K.L. Gurunatha, T.K. Maji. *Cryst. Growth Des.*, **9**, 4147 (2009).
[10] Y. Ma, A.L. Cheng, J.Y. Zhang, Q. Yue, E.Q. Gao. *Cryst. Growth Des.*, **9**, 867 (2009).
[11] W.Z. Shen, X.Y. Chen, P. Cheng, S.P. Yan, B. Zhai, D.Z. Liao, Z.H. Jiang. *Eur. J. Inorg. Chem.*, **2297**, (2005).
[12] P.-W. Liu, C.-P. Li, Y. Bi, J. Chen. *J. Coord. Chem.*, **66**, 2012 (2013).
[13] L.F. Ma, L.Y. Wang, M. Du, S.R. Batten. *Inorg. Chem.*, **49**, 365 (2009).
[14] E. Tynan, P. Jensen, N.R. Kelly, P.E. Kruger, A.C. Lees, B. Moubaraki, K.S. Murray. *Dalton Trans.*, 3440 (2004).
[15] H. He, D. Collins, F. Dai, X. Zhao, G. Zhang, H. Ma, D. Sun. *Cryst. Growth Des.*, **10**, 895 (2010).
[16] Y.X. Zhou, X.Q. Shen, C.X. Du, B.L. Wu, H.Y. Zhang. *Eur. J. Inorg. Chem.*, **4280**, (2008).
[17] C. Hou, Y. Zhao, T.-A. Okamura, P. Wang, W.-Y. Sun. *J. Coord. Chem.*, **65**, 4409 (2012).
[18] H.-W. Kuai, T.-A. Okamura, W.-Y. Sun. *J. Coord. Chem.*, **65**, 3147 (2012).
[19] Z.H. Cui, S.S. Wang, X.G. Wang, D.Z. Gao, Y.Q. Sun, G.Y. Zhang, Y.Y. Xu. *Z. Anorg. Allg. Chem.*, **638**, 669 (2012).
[20] X.F. Guo, X.J. Li, X.L. Weng, S. Lin. *J. Mol. Struct.*, **1008**, 63 (2012).
[21] G.X. Liu, X.F. Wang, H. Zhou. *Z. Anorg. Allg. Chem.*, **638**, 455 (2012).
[22] X.J. Li, R. Cao, W. Bi, Y. Wang, Y. Wang, X. Li, Z. Guo. *Cryst. Growth Des.*, **5**, 1651 (2005).
[23] X.J. Li, Y.Z. Cai, Z.L. Fang, L.J. Wu, B. Wei, S. Lin. *Cryst. Growth Des.*, **11**, 4517 (2011).
[24] S. Valiyaveettil, V. Enkelmann, K. Mullen. *Chem. Commun.*, **2097**, (1994).
[25] SHELXTLTM version 5, *Reference Manual*; Science Energy & Automation, Madison, WI (1994).
[26] M. Ruíz, L. Perelló, J. Server-Carrió, R. Ortiz, S. García-Granda, M.R. Díaz, E. Cantón. *J. Inorg. Biochem.*, **69**, 231 (1998).
[27] X.J. Li, R. Cao, W.H. Bi, Y.Q. Wang, Y.L. Wang, X. Li. *Polyhedron*, **24**, 2955 (2005).
[28] X.Y. Cao, J. Zhang, Z.J. Li, J.K. Cheng, Y.G. Yao. *Cryst. Eng. Comm.*, **9**, 806 (2007).
[29] L.F. Ma, Y.Y. Wang, J.Q. Liu, G.P. Yang, M. Du, L.Y. Wang. *Cryst. Eng. Comm.*, **111**, 1800 (2009).
[30] J.H. Qin, L.F. Ma, Y. Hu, L.Y. Wang. *Cryst. Eng. Comm.*, **14**, 2891 (2012).
[31] Z. Wang, Q. Wei, G. Xie, Q. Yang, S. Chen, S. Gao. *J. Coord. Chem.*, **65**, 286 (2012).
[32] S.L. Zheng, J.H. Yang, X.L. Yu, X.M. Chen, W.T. Wong. *Inorg. Chem.*, **43**, 830 (2004).
[33] X.X. Li, G.Y. Yang. *Chem. Eur. J.*, **17**, 13032 (2011).
[34] G. Aromi, A.J. Tasiopoulos, V. Nastopoulos, S.P. Perlepes. *Eur. J. Inorg. Chem.*, **18**, 2761 (2007).